# Configurational Entropy in Ice Nanosystems: Tools for Structure Generation and Screening

P. Parkkinen,* S. Riikonen, and L. Halonen

Laboratory of Physical Chemistry, Department of Chemistry, University of Helsinki, P.O. Box 55, FI-00014, Helsinki, Finland

**ABSTRACT:** Recently, a number of experimental and theoretical studies of low-temperature ice and water in nanoscale systems have emerged. Any theoretical study trying to model such systems will encounter the proton-disorder problem, i.e., there exist many configurations differing by water-molecule rotations for a fixed oxygen atom structure. An extensive search within the allowed proton-disorder space should always be performed to ensure a reasonable low-energy isomer and to address the effect of proton-configurational entropy that may affect experimental observables. In the present work, an efficient general-purpose program for finite,



semiperiodic, and periodic systems of hydrogen-bonded molecules is presented, which can be used in searching and enumerating the proton-configurational ensemble. Benchmarking tests are performed for ice nanotubes and finite slabs. Finally, the program is applied to experimentally appropriate ice nanosystems. A boron nitride film supported ice nanodot is studied in detail. Using a systematic generation of its proton-configurational ensemble, we find an isomer that is ~1 eV lower in total energy than one previously studied. The present isomer features a considerable dipole moment and implies that ice nanodots are inherently ferroelectric parallel to the surface. We conclude by demonstrating how the so-called hydrogen-bond connectivity parameters can be used to screen low-energy isomers.
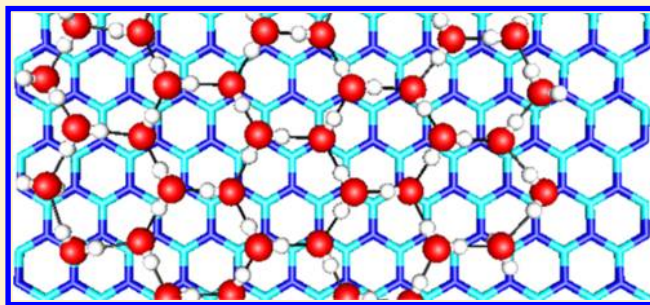
## ■ INTRODUCTION

One of the most fascinating yet complex properties of ice is its residual entropy, which arises from the large number of possible arrangements of the constituent water monomers.[1] Although Bernal-Fowler ice rules are fulfilled in an ice crystal,[2] a considerable amount of structural freedom still remains. The various structural isomers are referred to as "proton configurations", which constitute a statistical ensemble that can be surprisingly large. The number of possible configurations in hexagonal ice (ice-Ih) with $N$ molecules, was estimated by Pauling[3] to be $(3/2)^N$, while the exact number was later calculated to be $1.5069^N$.[4] The resulting entropy[4] of 3.410 J K$^{-1}$ beautifully fits the experimental value of $3.4 \pm 0.6$ J K$^{-1}$.[1]

Recently, there has been a surge in density functional theory (DFT) studies of water and ice at the atomic scale, facilitated by developments in algorithmic efficiency[5] and the treatment of the dispersion correction.[6−8] Experimental and theoretical studies of ice nanostructures, including ones formed on various surfaces and nanomaterials, continue to appear in the scientific literature. Systems of great interest include atomic layers of ice formed on silica and mica surfaces,[9−11] ice stripes and chains formed spontaneously on metals,[12−14] ice and low-temperature water/ice intercalated in epitaxial graphene,[10,11] ice "nanodots" grown on the hydrophilic boron nitride nanomesh,[15−17] and ice nanotubes formed inside carbon nanotubes[18−27] and inside other nanoporous media,[28] just to mention a few representative examples.

The complexity of proton disorder has been thoroughly discussed by the water cluster community,[29−40] and, con-

sequently, algorithms that determine the number of total proton configurations[41,42] or generate and screen energetically favorable isomers have been developed.[36,41−45] From the point of view of practical calculations, the large number of isomers is challenging. Even the water dodecahedron, which consists of only 20 water molecules and fullfils modified yet strict ice rules, has over 30 000 symmetry-independent proton configurations.[35] On the other hand, it has been shown that the most relevant low-energy isomers can be efficiently screened by the so-called hydrogen-bond connectivity parameters.[30−34,39] Systematic generation of the proton-configurational ensemble has also been performed for small bulk unit cells,[46−49] while for ice surfaces, Monte Carlo (MC) sampling techniques have been the method of choice.[50−52]

Although proton disorder is a well-established phenomenon of bulk ice and ice nanoclusters, it is omitted in many modern studies of ice nanostructures. Low-energy structures are a mandatory starting point for any density functional theory (DFT) or empirical molecular dynamics (MD) study. However, in many such studies, these isomers are not systematically searched from the proton-configurational ensemble. This is alarming, because choosing an incorrect isomer can result in a structure that may be over 1 eV (1 eV = 96.485 kJ/mol) higher in total energy than the minimum-energy isomer.[39,53] The proton configuration of any ice structure is also intimately linked to its total dipole moment,
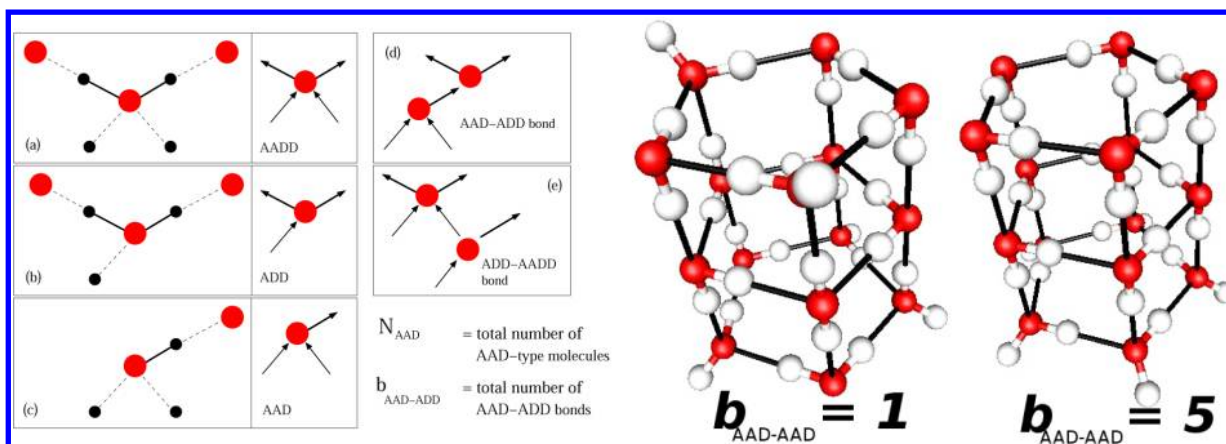
**Figure 1.** Explanatory figure of hydrogen-bond connectivity parameters, and an example of two systems with and identical oxygen raft but differing $b_{AAD\text{-}AAD}$ values.

which mandates its electrostatic interaction with the surroundings, further emphasizing the importance of finding the true low-energy isomers.

Ferroelectrocity in low-dimensional ice nanosystems has recently been discussed by several authors.[20,26] Dealing with ferroelectric phenomena in ice systems requires special care, as several, close-lying and competing proton-configurational isomers must be considered. To access the ferroelectric phenomena one should either (a) calculate the partition function by generating the proton-configurational ensemble (or a considerable part of it), or (b) perform Monte Carlo simulations within the ensemble. Unfortunately, for practical simulations, nonpolarizable empirical potentials (NPEPs) are not good enough in describing the subtle energetic differences between various microstates (isomers) and therefore cannot be used by such schemes.[23,54] Even for polarizable models, the relative energies can be sensitive to the parametrization of the model.[54] When it comes to standard MD simulations, even nanosecond-time scale simulations can fall short in sampling the complicated and "rugged"[55] energy landscape of proton disorder. On the other hand, graph invariants (or "hydrogen bond connectivity parameters") can be used in obtaining a robust, sub-kcal/mol (1 kcal/mol = 4.184 kJ/mol) per molecule accuracy fit to the energies obtained from DFT calculations. Such scheme, coupled with MC simulations, was successfully used by Singer et al.[49] to reproduce the ice-Ih/XI ferroelectric phase transition.

In the current work, we present an efficient and publicly available computer program for the generation, analysis, and prescreening of proton-configurational ensembles, which can handle finite, periodic, and semiperiodic (periodic only in one dimension or two dimensions) systems. It can be used in finding low-energy isomers, accessing the proton-configurational ensemble and thermodynamics and in deriving a total energy expression using hydrogen-bond connectivity parameters.

This work is organized as follows. First, in the Methods section, a brief introduction is given on hydrogen-bond connectivity parameters, followed by a detailed account of some novel ideas for ice structure generation and the details of DFT calculations. In the Results section, the code is first benchmarked with ice nanotubes and finite slabs, followed by an application to an ice nanodot/hexagonal boron nitride (h-BN) film system.

## METHODS

**Structure Classification and Screening.** For fast low-energy isomer searches and prescreening of proton configurations, the use of hydrogen-bond connectivity parameters[30,31,35,45] has been shown to work well for small water clusters[29,32−34,36,37,39] and bulk ice.[49] In the present work, we apply this approach to ice nanostructures. Some hydrogen-bond connectivity parameters are illustrated in Figure 1. We will take advantage mostly of $b_{AAD\text{-}AAD}$, $b_{DD\text{-}AD}$, etc. type parameters. Several studies on water clusters have determined that low-energy isomers tend to minimize parameters such as $b_{AAD\text{-}AAD}$ (i.e., the number of AAD−AAD hydrogen bonds).[34,37,39] This important piece of information makes it possible to judge energetics of icelike structures by a simple and fast visual inspection, while discarding structures featuring AAD-AAD bonds. For further details on graph invariants and connectivity parameters, the reader should consult refs 30, 31, 36, 37, and 45.

**Algorithm for Structure Generation.** In this section, we describe the implementation of our program and some new ideas that have been exploited. For earlier discussions on the problem of generating proton-configurational ensembles, see ref 36, as well as refs 43−45. The problem consists of distributing the hydrogen atoms between oxygen atoms, according to the Bernal-Fowler ice rules, and subsequently removing the symmetric results. The algorithm is recursive, and the $n$ configurations resulting from an iteration $j$ are given as an input for the iteration $j + 1$, excluding the first iteration ($j = 1$), for which an empty oxygen raft (no hydrogen atoms) of $N$ oxygen atoms is given as the only input structure ($n = 1$). Each iteration consists of the following operations:

(a) The possible water molecule orientations for oxygen atom $j$ are tested for $n$ given configurations. In the 3- or 4-fold coordinated molecules, there are six different configurations to place the two protons around the oxygen. For singly and doubly coordinated systems, there are, respectively, two and four possibilities to arrange the protons.

(b) The configurations breaking the ice rules are rejected. This is done by verifying that there is one and only one hydrogen between oxygen atom $j$ and its previously considered nearest neighbors.

(c) The symmetric results are removed from the generated configurations. In this step, symmetry operations of the

underlying oxygen raft are used to reduce the number of different structures.

(d) If the molecule considered is the last one (i.e., $j = N$), the execution is finished. Otherwise, the next oxygen atom ($j = j + 1$) is chosen from the raft. The resulting incomplete proton configurations of the current iteration are given as an input for the next, and the process is continued with operation (a).

The generation process can be illustrated as a tree (Figure 2), where each end of a branch (describing a partly filled proton
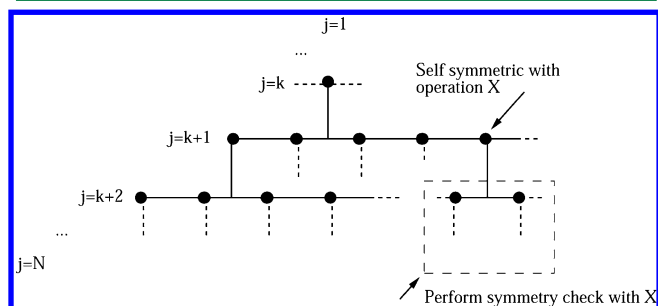


**Figure 2.** Inheritance tree of proton configurations. Each level of the tree corresponds to another iteration in the process, while the dots on the level $j$ have hydrogen atoms assigned to $j$ oxygens.

configuration) can generate up to six new branches (see step (a) above), until each structure has been divided $N$ times. The twigs at this level are the final proton configurations. The quick branching of the tree leads to a fast rise in the computational cost of the generation. In the following, the scalability of the process is discussed.

Operations (a) and (b) of the algorithm are straightforward and scale as O($n$). However, the symmetry check (operation (c)) is the most demanding part of the execution with the complexity of O($n^2$) in its simplest implementation. In this form, each structure found in the ice rules check and all proton configurations, resulting from the $M$ symmetry operations of the oxygen raft, must be compared against all other proton configurations. In the worst case, this results in a total of $36 \times n \times n \times (M - 1)$ comparisons. As the number of proton configurations, $n$, grows rapidly with increasing steps $j$, the number of performed operations becomes large. Graph invariants were introduced to overcome this problem in the symmetry check.[36,45] Graph invariants are properties of proton configurations that do not change when a symmetry operation is applied to the structure. Because of this, only the structures that possess the same graph invariant values can be symmetric with each other. This reduces the processing time requirement of the symmetry check from O($n^2$) to O($n \ln n$). Next, we introduce novel ways to make the proton configuration enumeration algorithm even more efficient, by further improving the symmetry check portion. Our improvements reduce the number of operations that must be executed during the symmetry check.

When a symmetry operation is applied to a structure, one water molecule is superposed onto another. Some symmetry operations can give meaningless results at a certain iteration step $j$, as the resulting structure does not have the hydrogen positions set for the same water molecules as the original. This is illustrated for a four-molecule square system after two iterations in Figure 3. Removing such void symmetry

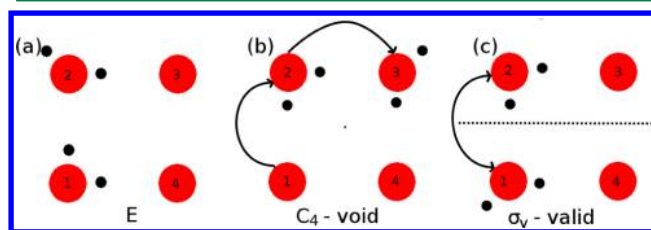operations results in a significant speedup for the symmetry checks.



**Figure 3.** Partly filled proton configuration of four molecule (square) system and two of its symmetries. (a) The original proton configuration, and proton configurations resulting from (b) a clockwise 90° rotation, and (c) a reflection with respect to a plane. The symmetry operation illustrated in panel (b) is meaningless for all proton configurations at this phase of iteration as water molecule 1 lacks the protons. The $\sigma_v$ operation (a reflection with respect to the $\sigma_v$ plane) on the other hand, is sensible, since both permuted molecules 1 and 2 have protons after the reflection operation.

The execution time can be reduced significantly once it is realized that, after the first testing of the symmetry operation $X$, two structures can be symmetric with each other via $X$ only if their "parent" structure (the structure from which they originate) is "self-symmetric" by the same operation. "Self-symmetric" means that the proton configuration resulting from a symmetry operation is identical with the initial configuration. This is illustrated in Figure 4, while the consequences of the
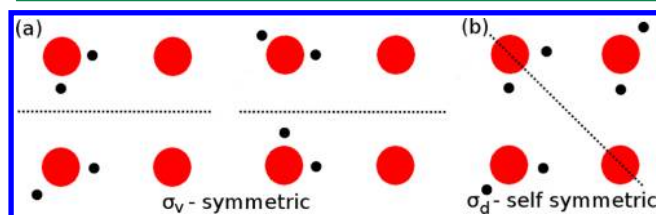


**Figure 4.** (a) Two $\sigma_v$ symmetric proton configurations of a four-molecule square system after two molecules are arranged and (b) a self-symmetric (with respect to $\sigma_d$) configuration after three iteration steps.
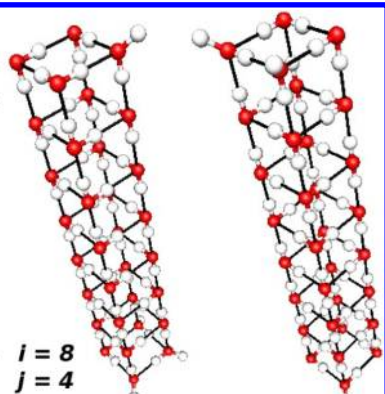
symmetry check on the treelike iterations are included in Figure 2: for a certain part of the iteration tree, symmetry checks with respect to the operation $X$ are necessary, as their parent-structure is self-symmetric in $X$.

We have implemented the algorithm in a freely available, easy-to-use program package. In addition, it allows the modification of many parameters of the enumeration and classification schemes. The program is highly optimized and is written in the Cython[56] programming language. The compiled program has a Python[57] interface in addition to the command line program. The NumPy,[58] Matplotlib,[59] and ASE[60] libraries are used. The symmetry operation search of periodic oxygen rafts takes advantage of SPGlib.[61,62] The symmetry search of nonperiodic systems is written according to instructions given in ref 63. The software is downloadable from the website[64] with detailed instructions.

**DFT Calculations.** All initial geometry optimizations were performed with the CP2K/Quickstep code[65] using the PBE exchange-correlation functional[66] and DZVP-molopt-SR (double-$\zeta$ valence polarized, molecularly optimized and short-range) basis sets.[67] Goedecker–Teter–Hutter pseudo-potentials[68]

**Table 1. Total Number of Proton Configurations in Ice Nanotubes of *i* Layers of *j* Molecule Rings**



| *i* | *j* = 4 | *j* = 5 | *j* = 6 | *j* = 7 |
|---|---|---|---|---|
| 3 | 178 | 860 | 4962 | 28896 |
| 4 | 978 | 7480 | 64835 | 580200 |
| 5 | 5588 | 66160 | 865243 | 149975872 |
| 6 | 33073 | 591328 | 11718758 | - |
| 7 | 198706 | 5321664 | - | - |
| 8 | 1210106 | 48112512 | - | - |
| 9 | 7434324 | - | - | - |
| 10 | 46016041 | - | - | - |

*i* = 8
*j* = 4

were utilized in describing the core electrons, while Grimme D3 corrections accounted for the dispersion.[7] Dipole moments of individual water monomers were extracted with the aid of Wannier function centers.[69] Systems were decoupled from their periodic images using the Martyna−Tuckerman scheme.[70] A few reoptimizations of low-energy isomers were performed with the GPAW[71,72] code, which is based on the real-space grid approach and, thus, does not suffer from spurious basis-set superposition errors. The PBE functional[66] was used in the GPAW calculations.

### ■ RESULTS

**Benchmarking: Ice Nanotubes and Finite Slabs.** Ice nanotubes (INTs) are ice clusters where *i* layers of *j* water molecule rings are stacked to form tubular structures. Some example structures with *j* = 4 are shown in Table 1, while two different proton configurations for the (*i* = 3, *j* = 5) case are illustrated in Figure 1. INTs are a prime example of water confined in nanoporous channels and of water in generally reduced dimensions. While theoretical calculations initially suggested the existence of INTs inside carbon nanotubes (CNTs),[18] their existence was later confirmed experimentally.[21,22] In the present work, finite INTs serve as a benchmark system for our method.

As a benchmark test, the complete proton-configurational ensembles for INTs of various tube diameters and lengths have been generated in Table 1. We reproduce the data previously calculated by Tokmachev and co-workers,[27] while we also explore larger and computationally more demanding systems. Figure 5 demonstrates the considerable speedup gained by the improvements implemented in our algorithm, reducing the amount of symmetry checks. Generating the (*i* = 8, *j* = 4) case and 1 210 106 configurations on a laptop, running on an Intel i5 vPro processor, takes ∼90 s with our most efficient algorithm. A natural application, following Singer, Kuo, and co-workers,[49] is to develop approximate energy expressions for INTs with the aid of connectivity parameters, a task which we performed in a previous work.[39] Such expressions can then be used in (a) generating the complete thermodynamical partition function[39] or (b) performing Monte Carlo dynamics[49] of the system. Our method certainly facilitates the systematic study of large INT/CNT systems in the future: lowest energy isomers can be searched while the entire ensemble can be generated to access INT thermodynamics and experimental observables, including INT ferroelectricity along the tube axis,[20,26] as a function of temperature.
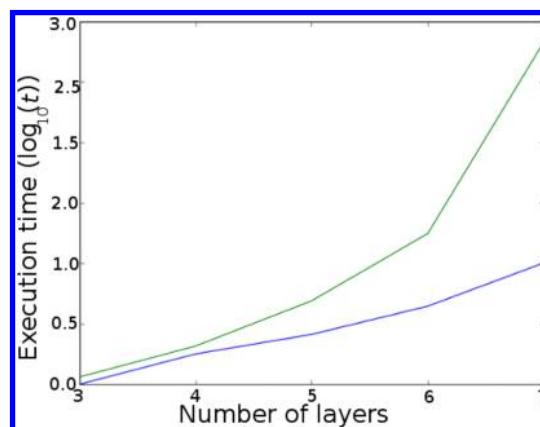


**Figure 5.** Logarithmic execution times of four-molecule ice nanotubes with different numbers of layers (*i* = 3, 4, 5, 6, 7) with (blue) and without (green) the separation of self-symmetric structures. The execution time for the three-layered nanotube is set to one.
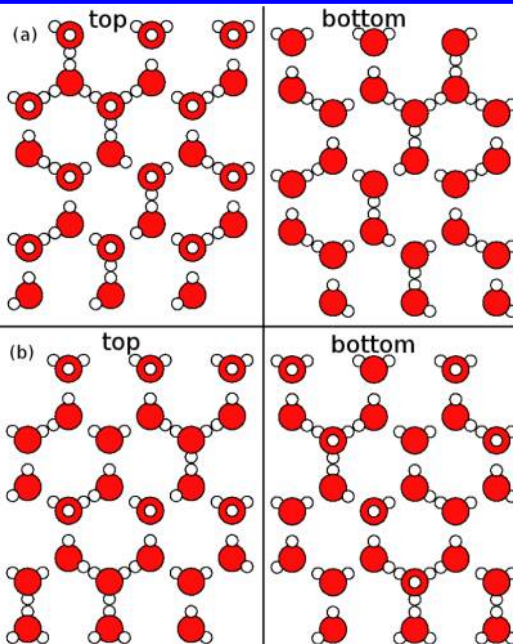
For large systems, the complete generation of proton configurational ensemble can quickly become intractable due to hardware limitations. In these cases, one might want to obtain only those proton configurations that have some desired features, e.g., dipole moments within a certain range or isomers possessing certain hydrogen-bond connectivity parameter values. Natural systems in this respect are finite slabs: for the ice-Ih basal plane, a reasonable constraint is to study systems featuring Fletcher-phase-like configurations only.[50,51,73] Our code allows this type of sampling, as, for example, some hydrogen bonds can be fixed to certain positions, or the number of a certain type of bonds (e.g., AAD−AAD) can be used as a constraint.

To benchmark constrained sampling of the proton-configurational ensemble, we used slabs of ice-Ih, consisting of multiples of the 8-molecule orthogonal cell.[43] They consisted of four double layers of Ice-Ih and hydrogen-bonding patterns on both sides of the slab were fixed, while the algorithm searched for all symmetry independent proton configurations within those fixed constraints. Two cases were studied: in the first, all dangling OH bonds on one vacuum-facing surface pointed along the surface normal (ferroelectric phase), while in the second case, different Fletcher-striped phases were fixed on both vacuum-facing surfaces.

The results of the systematic proton-configuration generation are listed in Table 2. According to Table 2, even for a rather moderate slab of 48 molecules and fixing the vacuum facing

**Table 2. Number of Symmetry-Independent Proton Configurations ($n$) in a Ferroelectric Ice Slab (Panel (a)), Having a Total of $N$ Water Molecules, and Different Fletcher Striped Phases (Panel (b))$^a$**



| $(n_x, n_y, n_z)$ | $N$ | $n$ |
|---|---|---|
| $(1, 1, 1)$ | 8 | 7 |
| $(2, 1, 1)$ | 16 | 15 |
| $(1, 1, 2)$ | 16 | 130 |
| $(2, 1, 2)$ | 32 | 893 |
| $(2, 1, 3)$ | 48 | 31701 |
| $(3, 1, 1)$ | 24 | 42 |
| $(3, 2, 1)$, system (a) | 48 | 541 |
| $(3, 2, 1)$, system (b) | 48 | 84390 |
| $(2, 2, 2)$ | 64 | 38579 |

$^a$The slabs are constructed as multiples of the minimal orthogonal unit cell, which has eight molecules arranged in two bilayers. This unit cell is repeated to $x$, $y$, and $z$ ($z$ normal to the surface) directions $n_x$, $n_y$, and $n_z$ times, respectively, resulting in a variety of slab thicknesses and sizes. For the $(3,2,1)$ case, a Fletcher striped phase is also considered: the structure tagged as "system (b)" has both of its vacuum-facing surfaces frozen in different Fletcher striped phases (visualized in panel (b)).

double layers, hundreds of thousands of bulk configurations arise. For the $(3, 2, 1)$ case, execution times of generation were 2.5 and 8.4 min for the ferroelectric (a) and Fletcher striped phase (b) cases, respectively. It is known that, for ice slabs of Ih basal plane, the total energy of the system is dominated by surface dangling OH-bond patterns.[50,51,73] Then, according to our analysis, even for a moderate size slab, such as the 48 molecule case studied here, for a certain surface OH-bond structure, there exist many (over 300 000) energetically almost degenerate proton configurations. According to our results, there is a strong entropic factor favoring the Fletcher-striped phase.

In the future, the systematic way of studying Ice-Ih surfaces demonstrated here can be applied to various systems, such as thin ice films on silica, mica, and to other similar cases,[9−11,74] while model systems for studying heterogeneous reactions on ice[75,76] can be generated with ease. An interesting question arises, for example, related to hydroxylated silica surfaces: the hydroxyl groups create strong hydrogen bonds to the first icelike layer, forcing the consecutive layers to form ferroelectric ice (similar to system (a) of Table 2). On the other hand, there must be a competition between (i) the hydroxyl water-molecule binding (which forces unfavorable ferroelectric phase) and (ii) favorable Fletcher-type phases, i.e., system (b) of Table 2. In the future, such problems can be studied with the aid of our code in a more realistic and systematic manner with relevant proton configurational isomers than has been done in some previous studies.[11,74]

**The Ice Nanodot.** Recently, nanoscopic ice clusters of circular shape have been synthesized[15−17] on the boron nitride nanomesh.[77,78] For this system, DFT calculations have also been performed. Initially a 42-water-molecule model geometry[15] was used in the calculations, while later, the same authors utilized a 38-molecule system,[17] as the exact number of water monomers is difficult to determine experimentally, because of the fast migration of molecules near the nanodot borders.[17] This system is ideal for studying the effects of proton disorder on energetics: it consists of a single bilayer of water molecules, while in the most-stable model system,[17] the bottom layer protons are hydrogen-bonded to the underlying nitrogen atoms. In ref 15, the proton configuration of the model system was based on the "minimum dipole moment" argument, and similar explanation was adopted in ref 17 for the minimum energy structure.

There are several intriguing questions regarding the nanodot system at low temperatures. How many proton configurations does this relatively small system have? Is there a single dominant low-energy isomer? Do the low-energy isomers feature a finite dipole moment, and, if so, how large is it? The latter question is important, as the dipole field mandates the electrostatic interaction of the nanodot with its surroundings (as emphasized by the authors of ref 15) and with neighboring nanodots. In ref 17, several model systems for the oxygen positions are considered, while, based on a few proton configurations only, their energetic differences are small. What are the energy differences of the lowest-energy isomers of each model system, once these isomers are searched from the proton-configurational ensemble? Near the energy minimum, do the proton-configurations of different oxygen-atom models become mixed in a similar fashion, as occurs in small water clusters?[39]

In the present work, we performed a proton-configurational analysis for the 42-molecule model system.[15] The role of the metal substrate was omitted, while an orthogonal supercell of monolayer h-BN with dimensions of 26.0 Å $\times$ 30.0 Å is used. In the calculations, h-BN is allowed to relax, resulting in a bending

1260

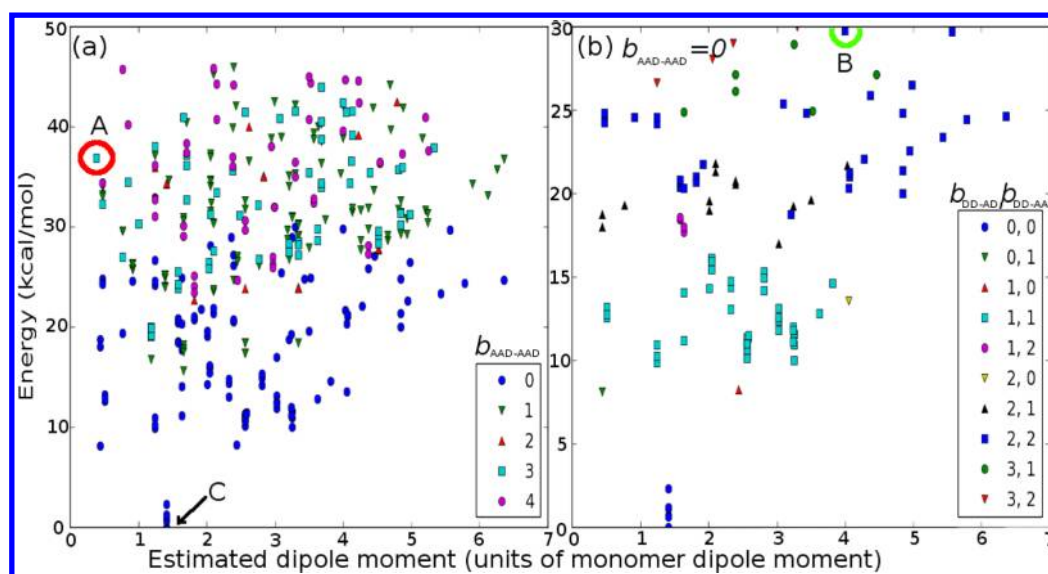dx.doi.org/10.1021/ct400931p | J. Chem. Theory Comput. 2014, 10, 1256−1264

**Figure 6.** Energetics of DFT optimized 16-molecule ice-nanodots (a) grouped by the value of $b_{AAD-AAD}$ and (b) ice nanodots with $b_{AAD-AAD} = 0$, further classified using $b_{DD-AD}$ and $b_{DD-AAD}$. The capital letters A, B, and C accompanied with a red circle, a green circle, and an arrow represent the example systems of Figures 7a−c.
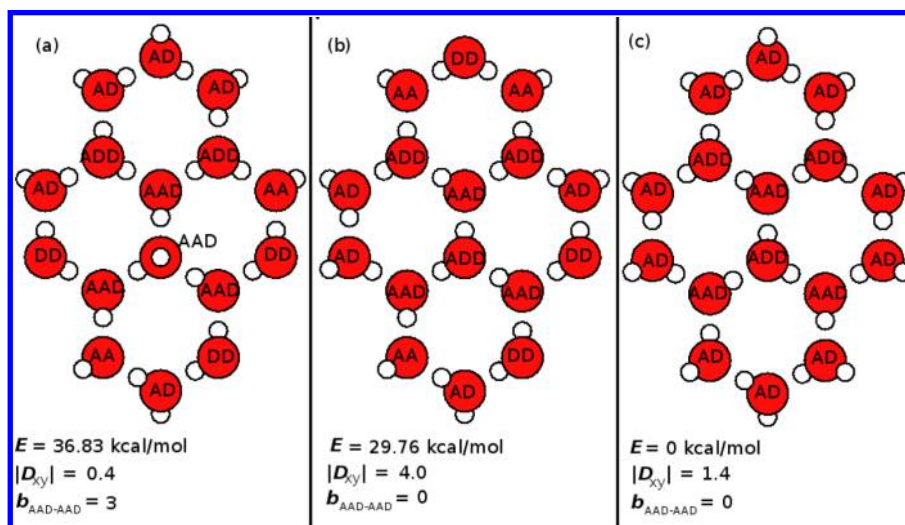


**Figure 7.** Three representative proton configurations of a 16-molecule ice-nanodot. Estimated dipole moments $|D_{xy}|$ are given in as multiples of the dipole moment of a single water monomer. The structures (a), (b), and (c) are marked in Figure 6 with a red circle, a green circle, and an arrow, respectively.

of the film under the water molecules. In order to find the energetically most stable isomer of the nanodot, we must first determine which connectivity parameters are critical for the total energy. This is important for any icelike structure having 3- or 2-fold coordinated molecules, because there is a considerable energy gap between systems exhibiting optimal and nonoptimal bonding parameters.[39] The magnitude of this gap ensures that only a few low-energy isomers must be considered. This is different from bulk ice where different configurations are energetically almost degenerate.[46] For the determination of optimal connectivity parameters, a small nanodot of 16 water molecules is employed, which, according to our analysis, features only a moderate number of 1800 proton configurations. Of the 1800 configurations, a few hundred randomly picked structures are reoptimized using DFT and the total energies are calculated.

We classify the structures according to the hydrogen-bond connectivity parameters, starting with $b_{AAD-AAD}$, i.e., the total number of AAD−AAD bonds. Such bonds have been found to dominate the energetics of isolated gas-phase clusters with 3- and 4-fold coordinated water molecules.[34,37,39] We observed that this is also the case for the nanodot studied here, as can be seen in Figure 6a, where the relative energies of the structures are plotted as a function of the dipole moment (an estimated dipole moment from the vector sum of individual water monomers). Colors on the scatter plot correspond to different $b_{AAD-AAD}$ values. A clear partition is observed: the structures with the lowest energies have the lowest $b_{AAD-AAD}$ value. To ensure that the minimum energy structure was taken in consideration, all the structures with such $b_{AAD-AAD}$ value were calculated and included in Figures 6a and 6b. Further classification of the $b_{AAD-AAD} = 0$ structures with the total amount of DD−AD, DD−AAD, and DD−AA bonds further
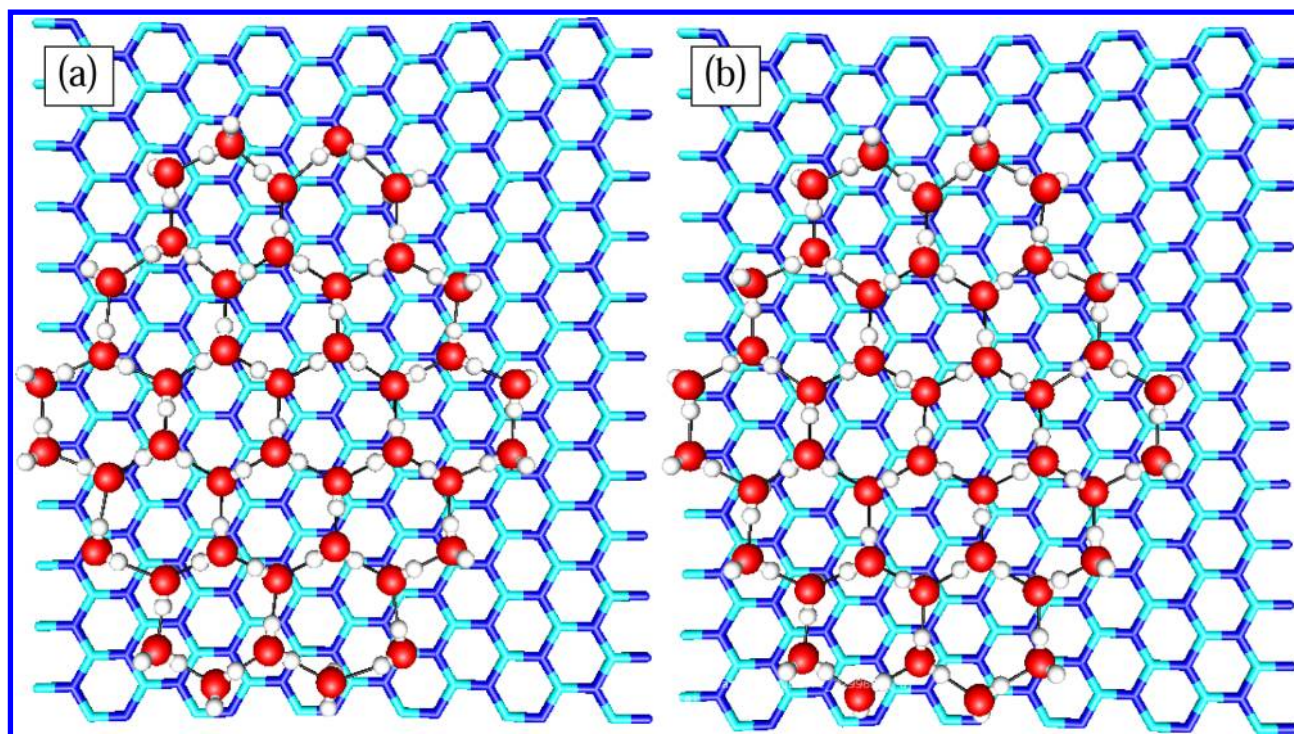
**Figure 8.** Two proton configurations of a 42-molecule ice-nanodot on a boron nitride film: (a) structure used by Ma et al.[15] and (b) representative of optimal hydrogen-bonding parameters.

reduces the number of minimum energy structure candidates (DD–AD and DD–AAD are presented in Figure 6b).

Figures 6a and 6b clearly show that there is no strong correlation with the energy of the system and its dipole moment. We emphasize that a high-energy isomer, far from the optimal structure, may be incorrectly chosen if one selects structures based only on the minimum of the dipole moment: in Figure 7, three representative cases have been chosen: (a) a system with a vanishing dipole moment, but with $b_{AAD-AAD} = 3$ and (b) and (c) two systems with a finite dipole moment but having $b_{AAD-AAD} = 0$. System (b) with a finite dipole moment is energetically more stable, by a total of 7.07 kcal/mol than the structure determined using system (a). System (c), which was selected based on the further classification, is the lowest-energy isomer, having a finite dipole moment (1.4 times the dipole moment of an individual water monomer). This configuration lies 36.83 kcal/mol lower in total energy than the minimum-dipole-moment system (system (a)).

Next, we recycled the hydrogen-bond parameters that worked for the 16-molecule nanodot and used them to screen low-energy isomers for the more-realistic 42-molecule case. We constrain the proton-configurational ensemble by requiring that $b_{AAD-AAD} = 0$, $b_{DD-AA} = 0$, $b_{DD-AAD} = 0$, and $b_{DD-AD} = 0$. Screening the ensemble this way reduces the number of minimum energy candidates to only 175 structures. After analyzing the structure used in ref 15, we observe that it has $b_{DD-AD} = 4$, $b_{DD-AAD} = 4$, and $b_{DD-AA} = 2$. After performing DFT geometry optimizations and total energy calculations, we find out that it lies 23.39 kcal/mol higher in energy than our optimal parameter isomer. The difference is 22.74 kcal/mol according to GPAW calculations. Both structures are presented in Figure 8. The lowest-energy isomer in Figure 8b has a total dipole moment of 13.76 D parallel to the surface (1 D = 3.33564 × 10⁻³⁰ C m), as obtained from DFT calculations. Interestingly, the hydrogen-bond connectivity parameters of the structure obtained here

with a systematic search are similar to those of the 38-molecule system of ref 17, when the singly coordinated molecule of the cited article is excluded. Furthermore, judging from the smaller 16-molecule model system and Figure 6, ice nanodots are inherently ferroelectric parallel to the surface as the minimum-energy basin is dominated by systems exhibiting considerable dipole moments. In future studies, the extent of ferroelectricity in the nanodot system can easily be explored using the tools described in this work, while the role of the metal surface should be addressed along the lines of refs 16 and 17.

## ■ CONCLUSIONS

An exhaustive analysis of the proton configurational ensemble is critical for density functional theory (DFT) studies of ice nanosystems, as realistic low-energy initial structures are needed, and entropic effects arising from proton disorder should be taken into account. Studying the thermodynamics of ice nanosystems calls for detailed knowledge of proton-configurational microstates in the vicinity of the energy minimum. In the present work, an efficient general purpose program for the generation, analysis, and screening of proton-configurational ensembles in ice nanosystems is presented and this program is made publicly available.[64] In addition, new ideas have been suggested to the proton configuration enumeration algorithm. The code has been benchmarked on some representative test systems.

Ice nanotubes form spontaneously inside carbon nano-tubes.[18,21,22] The simultaneous requirement of water molecule confinement and fullfilment of the ice rules results in the emergence of a net dipole moment along the tube axis.[20,26] The program presented in this work, being efficient for increasing ice nanotube lengths, allows for the systematic study of ferroelectric phases in ice nanotubes and similar systems. Finite slabs of the ice-Ih basal plane are known to favor Fletcher striped phases, while, contrary to this, many hydrophilic

surfaces, such as silica and mica, induce ferroelectric ordering along the slab normal. In the future, the code can be used in studying such problems, because, in this article, it was demonstrated to be efficient in the treatment of topologies with constrained surface hydrogen bonds. Proton configurations in the ice nanodot/hexagonal boron nitride nanomesh[15−17] were systematically studied and hydrogen-bond connectivity parameters were demonstrated to work as effective screening parameters for this system, facilitating theoretical studies on this system in the future. We have also emphasized the inherent ferroelectricity of this system.

Since the number of experimental and theoretical studies of low-temperature ice nanostructures formed on various nanomaterials is increasing in the literature, we hope that the code made available in this work will facilitate the interpretation and analysis of such studies. In addition, we hope that our work will improve the quality of ice-related calculations by offering the means to obtain more-realistic model systems.

## ■ AUTHOR INFORMATION

**Corresponding Author**

*E-mail: pauli.parkkinen@helsinki.fi.

**Notes**

The authors declare no competing financial interest.

## ■ ACKNOWLEDGMENTS

## ■ REFERENCES

(1) Giauque, W. F.; Stout, J. W. The Entropy of Water and the Third Law of Thermodynamics. The Heat Capacity of Ice from 15 to 273 K. *J. Am. Chem. Soc.* **1936**, *58*, 1144−1150.

(2) Bernal, J. D.; Fowler, R. H. A Theory of Water and Ionic Solution, with Particular Reference to Hydrogen and Hydroxyl Ions. *J. Chem. Phys.* **1933**, *1*, 515−548.

(3) Pauling, L. The Structure and Entropy of Ice and of Other Crystals with Some Randomness of Atomic Arrangement. *J. Am. Chem. Soc.* **1935**, *57*, 2680−2684.

(4) Nagle, J. F. Lattice Statistics of Hydrogen Bonded Crystals. I. The Residual Entropy of Ice. *J. Math. Phys.* **1966**, *7*, 1484−1491.

(5) VandeVondele, J.; Hutter, J. An efficient orbital transformation method for electronic structure calculations. *J. Chem. Phys.* **2003**, *118*, 4365−4369.

(6) Tkatchenko, A.; Scheffler, M. Accurate Molecular Van Der Waals Interactions from Ground-State Electron Density and Free-Atom Reference Data. *Phys. Rev. Lett.* **2009**, *102*, 073005.

(7) Grimme, S.; Antony, J.; Ehrlich, S.; Krieg, H. A Consistent and Accurate *ab initio* Parametrization of Density Functional Dispersion Correction (DFT-D) for the 94 Elements H-Pu. *J. Chem. Phys.* **2010**, *132*, 154104.

(8) Lee, K.; Murray, E. D.; Kong, L.; Lundqvist, B. I.; Langreth, D. C. Higher-accuracy van der Waals density functional. *Phys. Rev. B* **2010**, *82*, 081101.

(9) Bluhm, H.; Salmeron, M. Growth of nanometer thin ice films from water vapor studied using scanning polarization force microscopy. *J. Chem. Phys.* **1999**, *111*, 6947−6954.

(10) Xu, K.; Cao, P.; Heath, J. R. Graphene Visualizes the First Water Adlayers on Mica at Ambient Conditions. *Science* **2010**, *329*, 1188−1191.

(11) Li, H.; Zeng, X. C. Two Dimensional Epitaxial Water Adlayer on Mica with Graphene Coating: An ab Initio Molecular Dynamics Study. *J. Chem. Theory Comput.* **2012**, *8*, 3034−3043.

(12) Cerdá, J.; Michaelides, A.; Bocquet, M.-L.; Feibelman, P. J.; Mitsui, T.; Rose, M.; Fomin, E.; Salmeron, M. Novel Water Overlayer Growth on Pd(111) Characterized with Scanning Tunneling Microscopy and Density Functional Theory. *Phys. Rev. Lett.* **2004**, *93*, 116101.

(13) Yamada, T.; Tamamori, S.; Okuyama, H.; Aruga, T. Anisotropic Water Chain Growth on Cu(110) Observed with Scanning Tunneling Microscopy. *Phys. Rev. Lett.* **2006**, *96*, 036105.

(14) Carrasco, J.; Michaelides, A.; Forster, M.; Haq, S.; Raval, R.; Hodgson, A. A one-dimensional ice structure built from pentagons. *Nat. Mater.* **2009**, *8*, 427−431.

(15) Ma, H.; Brugger, T.; Berner, S.; Ding, Y.; Iannuzzi, M.; Hutter, J.; Osterwalder, J.; Greber, T. Nano-ice on Boron Nitride Nanomesh: Accessing Proton Disorder. *ChemPhysChem* **2010**, *11*, 399−403.

(16) Ding, Y.; Iannuzzi, M.; Hutter, J. Investigation of Boron Nitride Nanomesh Interacting with Water. *J. Phys. Chem. C* **2011**, *115*, 13685−13692.

(17) Ding, Y.; Iannuzzi, M.; Hutter, J. Nano-ice models for the water aggregates observed on the h-BN/Rh(111) nanomesh. *J. Phys.: Condens. Matter* **2012**, *24*, 445002.

(18) Koga, K.; Gao, G.; Tanaka, H.; Zeng, X. Formation of ordered ice nanotubes inside carbon nanotubes. *Nature* **2001**, *412*, 802.

(19) Bai, J.; Wang, J.; Zeng, X. C. Multiwalled ice helixes and ice nanotubes. *Proc. Natl. Acad. Sci. U.S.A.* **2006**, *103*, 19664−19667.

(20) Luo, C.; Fa, W.; Zhou, J.; Dong, J.; Zeng, X. C. Ferroelectric Ordering in Ice Nanotubes Confined in Carbon Nanotubes. *Nano Lett.* **2008**, *8*, 2607−2612.

(21) Maniwa, Y.; Kataura, H.; Abe, M.; Udaka, A.; Suzuki, S.; Achiba, Y.; Kira, H.; Matsuda, K.; Kadowaki, H.; Okabe, Y. Ordered water inside carbon nanotubes: formation of pentagonal to octagonal ice-nanotubes. *Chem. Phys. Lett.* **2005**, *401*, 534−538.

(22) Byl, O.; Liu, J.-C.; Wang, Y.; Yim, W.-L.; Johnson, J. K.; Yates, J. T. Unusual Hydrogen Bonding in Water-Filled Carbon Nanotubes. *J. Am. Chem. Soc.* **2006**, *128*, 12090−12097.

(23) Bai, J.; Su, C.-R.; Parra, R. D.; Zeng, X. C.; Tanaka, H.; Koga, K.; Li, J.-M. Ab initio studies of quasi-one-dimensional pentagon and hexagon ice nanotubes. *J. Chem. Phys.* **2003**, *118*, 3913−3916.

(24) Agrawal, B. K.; Singh, V.; Pathak, A.; Srivastava, R. *Ab initio* study of ice nanotubes in isolation or inside single-walled carbon nanotubes. *Phys. Rev. B* **2007**, *75*, 195420.

(25) Kurita, T.; Okada, S.; Oshiyama, A. Energetics of ice nanotubes and their encapsulation in carbon nanotubes from density-functional theory. *Phys. Rev. B* **2007**, *75*, 205424.

(26) Mikami, F.; Matsuda, K.; Kataura, H.; Maniwa, Y. Dielectric Properties of Water inside Single-Walled Carbon Nanotubes. *ACS Nano* **2009**, *3*, 1279−1287.

(27) Tokmachev, A. M.; Dronskowski, R. Hydrogen-bond Networks in Finite Ice Nanotubes. *J. Comput. Chem.* **2011**, *32*, 99−105.

(28) Zhao, H.-X.; Kong, X.-J.; Li, H.; Jin, Y.-C.; Long, L.-S.; Zeng, X. C.; Huang, R.-B.; Zheng, L.-S. Transition from one-dimensional water to ferroelectric ice within a supramolecular architecture. *Proc. Natl. Acad. Sci. U.S.A.* **2011**, *108*, 3481−3486.

(29) Lenz, A.; Ojamae, L. A Theoretical Study ofWater Clusters: the Relation between Hydrogenbond Topology and Interaction Energy from Quantum-chemical Computations for Clusters with up to 22 Molecules. *Phys. Chem. Chem. Phys.* **2005**, *7*, 1905−1911.

(30) Anick, D. J. Polyhedral Water Clusters, I: Formal Consequences of the Ice Rules. *J. Mol. Struct.: THEOCHEM* **2002**, *587*, 87−96.

(31) Anick, D. J. Polyhedral Water Clusters, II: Correlations of Connectivity Parameters with Electronic Energy and Hydrogen Bond Lengths. *J. Mol. Struct.: THEOCHEM* **2002**, *587*, 97−110.

(32) Anick, D. J. Application of database methods to the prediction of B3LYP-optimized polyhedral water cluster geometries and electronic energies. *J. Chem. Phys.* **2003**, *119*, 12442−12456.

(33) Anick, D. J. Zero Point Energy of Polyhedral Water Clusters. *J. Phys. Chem. A* **2005**, *109*, 5596−5601.

(34) Anick, D. J. Topology-energy Relationships and Lowest Energy Configurations for Pentagonal Dodecahedral $(H_2O)_{20}X$ clusters, X =

1263

dx.doi.org/10.1021/ct400931p | *J. Chem. Theory Comput.* 2014, 10, 1256−1264

empty, H$_2$O, NH$_3$, H$_3$O$^+$: The Importance of O-topology. *J. Chem. Phys.* **2010**, *132*, 164311.

(35) McDonald, S.; Ojamäe, L.; Singer, S. J. Graph Theoretical Generation and Analysis of Hydrogen-Bonded Structures with Applications to the Neutral and Protonated Water Cube and Dodecahedral Clusters. *J. Phys. Chem. A* **1998**, *102*, 2824−2832.

(36) Kuo, J.; Ciobanu, C.; Ojamäe, L.; Shavitt, I.; Singer, S. Short H-bonds and Spontaneous Self-dissociation in (H$_2$O)$_{20}$: Effects of H-bond Topology. *J. Chem. Phys.* **2003**, *118*, 3583−3588.

(37) Kirov, M. V.; Fanourgakis, G. S.; Xantheas, S. S. Identifying the Most Stable Networks in Polyhedral Water Clusters. *Chem. Phys. Lett.* **2008**, *461*, 180−188.

(38) Lenz, A.; Ojamäe, L. A Theoretical Study of Water Equilibria: The Cluster Distribution Versus Temperature and Pressure for (H$_2$O)$_n$, n = 1−60, and Ice. *J. Chem. Phys.* **2009**, *131*, 134302.

(39) Parkkinen, P.; Riikonen, S.; Halonen, L. H$_2$O)$_{20}$ Water Clusters at Finite Temperatures. *J. Phys. Chem. A* **2013**, *117*, 9985−9998.

(40) Yoo, S.; Kirov, M. V.; Xantheas, S. S. Low-Energy Networks of the T-Cage (H$_2$O)$_{24}$ Cluster and Their Use in Constructing Periodic Unit Cells of the Structure I (sI) Hydrate Lattice. *J. Am. Chem. Soc.* **2009**, *131*, 7564−7566.

(41) Kirov, M. Residual entropy of polyhedral water clusters. Exact relations. *J. Struct. Chem.* **1994**, *35*, 126−128.

(42) Kirov, M. The transfer-matrix and max-plus algebra method for global combinatorial optimization: Application to cyclic and polyhedral water clusters. *Physica A* **2009**, *388*, 1431−1445.

(43) Hayward, J. A.; Reimers, J. R. Unit cells for the simulation of hexagonal ice. *J. Chem. Phys.* **1997**, *106*, 1518−1529.

(44) Lekner, J. Energetics of hydrogen ordering in ice. *Physica B* **1998**, *252*, 149−159.

(45) Kuo, J.; Coe, J.; Singer, S.; Band, Y.; Ojamäe, L. On the use of graph invariants for efficiently generating hydrogen bond topologies and predicting physical properties of water clusters and ice. *J. Chem. Phys.* **2001**, *114*, 2527−2540.

(46) Hirsch, T. K.; Ojamäe, L. Quantum-Chemical and Force-Field Investigations of Ice Ih: Computation of Proton-Ordered Structures and Prediction of Their Lattice Energies. *J. Phys. Chem. B* **2004**, *108*, 15856−15864.

(47) Kuo, J.-L.; Klein, M. L.; Kuhs, W. F. The effect of proton disorder on the structure of ice-Ih: A theoretical study. *J. Chem. Phys.* **2005**, *123*, 134505.

(48) Kuo, J.-L. The low-temperature proton-ordered phases of ice predicted by ab initio methods. *Phys. Chem. Chem. Phys.* **2005**, *7*, 3733−3737.

(49) Singer, S. J.; Kuo, J.-L.; Hirsch, T. K.; Knight, C.; Ojamäe, L.; Klein, M. L. Hydrogen-Bond Topology and the Ice VII/VIII and Ice Ih/XI Proton-Ordering Phase Transitions. *Phys. Rev. Lett.* **2005**, *94*, 135701.

(50) Buch, V.; Groenzin, H.; Li, I.; Shultz, M. J.; Tosatti, E. Proton Order in the Ice Crystal Surface. *Proc. Natl. Acad. Sci. U.S.A.* **2008**, *105*, 5969−5974.

(51) Pan, D.; Liu, L.-M.; Tribello, G. A.; Slater, B.; Michaelides, A.; Wang, E. Surface Energy and Surface Proton Order of the Ice Ih Basal and Prism Surfaces. *J. Phys.: Condens. Matter* **2010**, *22*, 074209.

(52) Sun, Z.; Pan, D.; Xu, L.; Wang, E. Role of Proton Ordering in Adsorption Preference of Polar Molecule on Ice Surface. *Proc. Natl. Acad. Sci. U.S.A.* **2012**, *109*, 13177−13181.

(53) Parkkinen, P.; Riikonen, S.; Halonen, L. Global Minima of Protonated Water Clusters (H$_2$O)$_{20}$H$^+$ Revisited. *J. Phys. Chem. A* **2012**, *116*, 10826−10835.

(54) Buch, V.; Sandler, P.; Sadlej, J. Simulations of H$_2$O Solid, Liquid, and Clusters, with an Emphasis on Ferroelectric Ordering Transition in Hexagonal Ice. *J. Phys. Chem. B* **1998**, *102*, 8641−8653.

(55) Wales, D. J.; Hodges, M. P. Global minima of water clusters (H$_2$O)$_n$, n ≤ 21, described by an empirical potential. *Chem. Phys. Lett.* **1998**, *286*, 65−72.

(56) Behnel, S.; Bradshaw, R.; Citro, C.; Dalcin, L.; Seljebotn, D.; Smith, K. Cython: The Best of Both Worlds. *Comput. Sci. Eng.* **2011**, *13*, 31−39.

(57) van Rossum, G. Scripting the Web with Python. *World Wide Web J.* **1997**, *2*, 97−120.

(58) Oliphant, T. E. Python for Scientific Computing. *Comput. Sci. Eng.* **2007**, *9*, 10−20.

(59) Hunter, J. D. Matplotlib: A 2D Graphics Environment. *Comput. Sci. Eng.* **2007**, *9*, 90−95.

(60) Bahn, S. R.; Jacobsen, K. W. An object-oriented scripting interface to a legacy electronic structure code. *Comput. Sci. Eng.* **2002**, *4*, 56−66.

(61) Grosse-Kunstleve, R. W. Algorithms for deriving crystallographic space-group information. *Acta Crystallogr., Sect. A: Found. Crystallogr.* **1999**, *55*, 383−395.

(62) Grosse-Kunstleve, R. W.; Adams, P. D. Algorithms for deriving crystallographic space-group information. II. Treatment of special positions. *Acta Crystallogr., Sect. A: Found. Crystallogr.* **2002**, *58*, 60−65.

(63) Largent, R. J.; Polik, W. F.; Schmidt, J. R. Symmetrizer: Algorithmic determination of point groups in nearly symmetric molecules. *J. Comput. Chem.* **2012**, *33*, 1637−1642.

(64) Ice Package V1.0. A general purpose program for generation and analysis of proton configurations. Available via the Internet at http://www.helsinki.fi/kemia/fysikaalinen/icepackage/, accessed Jan. 1, 2014.

(65) VandeVondele, J.; Krack, M.; Mohamed, F.; Parrinello, M.; Chassaing, T.; Hutter, J. Quickstep: Fast and Accurate Density Functional Calculations Using a Mixed Gaussian and Plane Waves Approach. *Comput. Phys. Commun.* **2005**, *167*, 103−128.

(66) Perdew, J. P.; Burke, K.; Ernzerhof, M. Generalized Gradient Approximation Made Simple. *Phys. Rev. Lett.* **1996**, *77*, 3865−3868.

(67) VandeVondele, J.; Hutter, J. Gaussian Basis Sets for Accurate Calculations on Molecular Systems in Gas and Condensed Phases. *J. Chem. Phys.* **2007**, *127*, 114105.

(68) Goedecker, S.; Teter, M.; Hutter, J. Separable Dual-space Gaussian Pseudopotentials. *Phys. Rev. B* **1996**, *54*, 1703−1710.

(69) Silvestrelli, P. L.; Parrinello, M. Water Molecule Dipole in the Gas and in the Liquid Phase. *Phys. Rev. Lett.* **1999**, *82*, 3308−3311.

(70) Martyna, G. J.; Tuckerman, M. E. A Reciprocal Space Based Method for Treating Long Range Interactions in *ab initio* and Force-field-based Calculations in Clusters. *J. Chem. Phys.* **1999**, *110*, 2810−2821.

(71) Mortensen, J. J.; Hansen, L. B.; Jacobsen, K. W. Real-space grid implementation of the projector augmented wave method. *Phys. Rev. B* **2005**, *71*, 035109.

(72) Enkovaara, J.; Rostgaard, C.; Mortensen, J. J.; Chen, J.; Dułak, M.; Ferrighi, L.; Gavnholt, J.; Glinsvad, C.; Haikola, V.; Hansen, H. A.; et al. Electronic structure calculations with GPAW: A real-space implementation of the projector augmented-wave method. *J. Phys.: Condens. Matter* **2010**, *22*, 253202.

(73) Fletcher, N. H. Surface structure of water and ice. *Philos. Mag.* **1968**, *18*, 1287−1300.

(74) Chen, Y.-W.; Chu, I.-H.; Wang, Y.; Cheng, H.-P. Water thin film-silica interaction on a-quartz (0001) surfaces. *Phys. Rev. B* **2011**, *84*, 155444.

(75) Riikonen, S.; Parkkinen, P.; Halonen, L.; Gerber, R. B. Ionization of Nitric Acid on Crystalline Ice: The Role of Defects and Collective Proton Movement. *J. Phys. Chem. Lett.* **2013**, *4*, 1850−1855.

(76) Murdachaew, G.; Gaigeot, M.-P.; Halonen, L.; Gerber, R. B. Dissociation of HCl into Ions on Wet Hydroxylated (0001) α-Quartz. *J. Phys. Chem. Lett.* **2013**, 3500−3507.

(77) Laskowski, R.; Blaha, P.; Gallauner, T.; Schwarz, K. Single-Layer Model of the Hexagonal Boron Nitride Nanomesh on the Rh(111) Surface. *Phys. Rev. Lett.* **2007**, *98*, 106802.

(78) Berner, S.; Corso, M.; Widmer, R.; Groening, O.; Laskowski, R.; Blaha, P.; Schwarz, K.; Goriachko, A.; Over, H.; Gsell, S.; et al. Boron Nitride Nanomesh: Functionality from a Corrugated Monolayer. *Angew. Chem.* **2007**, *119*, 5207−5211.